2-8

Evaluation of ERTS-1 Image Sensor Spatial Resolution in Photographic Form

R. A. Schowengerdt

P. N. Slater

Type II

Progress Report 3

Prepared for

NASA/ERTS Contract Number NAS5-21849

Proposal Number 618

Principal Investigator

P. N. Slater (UN237)

March 1973

TABLE OF CONTENTS

Section 1

INTRODUCTION AND SUMMARY

This report describes progress to date on contract number NAS5-21849 entitled "Evaluation of ERTS-1 Image Sensor Resolution in Photographic Form". The work described was carried out during the first six months of the contract from 1 September 1972 to 1 March 1973.

In the first part of this report we describe an analysis of the multispectral scanner (MSS) imagery in which a coherent optical system was used to display the spatial frequency content of the amplitude image.

The second part of this report deals with work preliminary to the microdensitometric scanning of near-simultaneous MSS and high altitude aircraft (A/C) imagery for the determination of the Optical Transfer Function (OTF) of the MSS for its four bands. The status of the data acquisition and analysis is described and some restrictions we have encountered are mentioned. The basic theory for this analysis procedure has recently been presented at the IX Congress of the International Commission for Optics in a paper entitled "Determination of the Inflight OTF of Orbital Earth Resources Sensors". A copy of this paper is included as an appendix to this report.

Author Identified Significant Results

A coherent optical system was used to display the spatial frequency content of the amplitude image* of one area of the ground as obtained in the four wavelength bands of the multispectral scanner (MSS). This enabled a rapid comparison to be made between the four bands, from which it was clear

*Note a coherent, laser illuminated optical system analyses the amplitude and phase transmission rather than the intensity transmission of a photographic image.

that bands 5 and 7 were preferred to the others in terms of image definition, and thus mapping and acreage estimation, for the particular agricultural area imaged.

With suitable scaling it was also possible to compare the modulation, as a function of spatial frequency, of MSS bands 4 and 5 with the green (BB) and red (DD) bands of the same area from the Apollo 9, S065 experiment. A significant result is that the modulation in the MSS amplitude imagery is 65% - 90% of that in the Apollo 9 amplitude imagery. In addition, the ratio of spatial frequencies for the ERTS and Apollo imagery, at which the same modulation occurs, lies between 0.55 and 0.75 for the red band. This ratio is closely related to the ratio of "resolutions" for the two sensors. These values corroborate statements[1] that the resolution of the MSS imagery is better than anticipated by pre-flight predictions.[2]

[1]S. C. Freden, "Introduction: Performance of Sensors and Systems", Earth Resources Technology Satellite-1 Symposium Proceedings, September 29, 1972.

[2]A. P. Colvocoresses, "Image Resolutions for ERTS, SKYLAB and GEMINI/APOLLO," Photogrammetric Engineering, 38 (1): 33-35, January 1972.

Section 2

COHERENT OPTICAL FOURIER ANALYSIS

Comparison Between ERTS-1 and Apollo 9 Imagery

Optical Fourier analysis[3] has been used to obtain relative comparisons between ERTS-1 bands 4 and 5 and the Apollo 9 S065 experiment's bands BB and DD. The optical bench arrangement used is shown below.

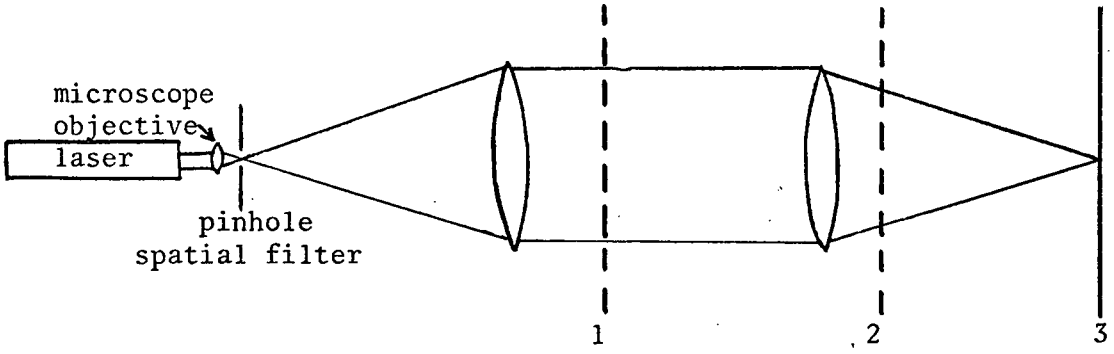

Optical Fourier Transform Set-up

If a photographic transparency is placed in plane 1, the Fourier transform of the transparency will appear in plane 3. Since the above system is using coherent light, the Fourier transform is performed on the complex amplitude transmission of the transparency. For a transparency with no phase relief or scratches, the amplitude transmission is real (i.e. not complex) and is the square root of the intensity transmission.

Thus, if the transparency has an amplitude transmission given by $t(x_1,y_1)$, the distribution of light in plane 3 is,

$$E_3(x_3,y_3) \sim |\tilde{t}|^2 \sim |FT[t(x_1,y_1)]|^2 \qquad \text{(scaling ignored)} \qquad (1)$$

where FT denotes the Fourier transform. By placing the transparency in plane 2 the scale of the Fourier transform can be adjusted by moving plane 2 relative to plane 3.

Note that the spatial frequency spectrum obtained above is not identical to that obtained by, say, Fourier transforming digital microdensitometer data. In that case, one is transforming the intensity transmission, T, of the transparency,

$$\tilde{T} \sim FT[T(x,y)]$$
$$= FT[t^2(x,y)] \quad (2)$$

Generally, (1) and (2) are two distinct functions and one cannot be obtained from the other.

A frame was selected from each set of imagery such that the ERTS and Apollo 9 coverage overlapped. The ERTS frame is diagrammed in Fig. 1, the circular area being the region which was transformed. Scaling was performed on the ERTS images to make the ground spatial frequency correspond to the Apollo 9 scale. Prints of the spectra obtained are shown in Fig. 2. The following points can be deduced immediately:

1) The vertical spikes in all cases are due to scratches on the film.
2) The horizontal spikes and dots in the ERTS frame are due to the lines present in the ERTS images, which are caused by faulty calibration of one detector (see section on Scan Lines).
3) The dots, most easily seen in the spectrum of Apollo 9, band DD, are due to the periodic square-wave nature of the agricultural fields indicated in Fig. 1. These dots can also be detected in the original photographs of the ERTS spectra at an angle of about 5° to the scan line spikes.

Fig. 3 shows microdensitometer scans of the original spectra transparencies along the azimuthal direction discussed in (3) above. The spectrum in each case was averaged about the origin to obtain these curves.

The data in Figs. 2 and 3 contain the experimental artifact of conversion from exposure to density in the step of photographically recording the spectra. The densities at selected frequencies were converted to relative exposures by using the D-log E curve for the processing of the spectra photography. The amplitude transmission modulation of the original image was then calculated at each frequency by the equation,

$$m_a(f) \sim \sqrt{E(f)/T_o} \tag{3}$$

where E is the relative exposure in the spectrum at the given frequency and T_o is the average intensity transmission of the area (indicated in Fig. 1) transformed. This formulation was based in the following model. Assume the transparency has an amplitude transmission given by,

$$t(x) = t_o + a_1 \cos 2\pi f_1 x \tag{4}$$

The amplitude transmission modulation is then,

$$m_a = 2a_1/t_o \tag{5}$$

The Fourier transform is taken optically to obtain,

$$\tilde{t}(f) = t_o\delta(f) + \frac{a_1}{2}\,\delta(f \pm f_1) \tag{6}$$

The intensity is recorded to give,

$$E(f) = |\tilde{t}(f)|^2 = t_o^2\delta(f) + \frac{a_1^2}{4}\,\delta(f \pm f_1) \tag{7}$$

Since, assuming no phase effects in the image,

$$T_o = t_o^2$$

we have eq. (3).

The resulting curves are shown in Fig. 4. They indicate a true reduction in spatial frequency content between the Apollo 9, band DD, and ERTS-1, band 5. Apollo 9, band BB, and ERTS-1, band 4, are more similar in spatial frequency content, indicating that this band may be limited in resolution by modulation reduction from atmospheric scattering, (or in this case, by the scene modulation in the green) rather than by sensor resolution or data processing.

A number closely related to the ratio of resolution between the ERTS and Apollo 9 sensors can be obtained in the following way. It is reasonable to assume that the spatial frequency at the resolution limit will have a fixed modulation, independent of the particular image. Therefore, lines of constant modulation were drawn on Fig. 4 , and the spatial frequency at which they crossed the ERTS and Apollo 9 spectra, were noted. The ratio of frequencies, for the same modulation, betweeen the two images is plotted in Fig. 5 . From these curves one can say there is a reduction in ground resolution (defined in this way) from Apollo 9 SO65 to ERTS of 0.7 - 0.9 for the green band and 0.55 - 0.75 for the red band.

The following qualifications apply to comparisons between the ERTS-1 and Apollo 9 imagery:

1) The spectral bands are not identical.
2) The imagery was taken at different times of day and 3 1/2 years apart.
3) The imagery examined are only single examples, subject to particular exposure and processing conditions.

Nevertheless, the comparisons are useful in establishing a base line for image information content.

Comparison Between ERTS Bands

Two microdensitometer scans were made for this comparison. One is the data

obtained above and is shown, for all ERTS bands, in Fig. 6. Again the amplitude transmission modulation is plotted versus spatial frequency. The red band (5) shows the highest spatial frequency content.

A more discriminating comparison was obtained by calculating the modulation corresponding to the frequency components of the agricultural field patterns (see point 3 page 4. These components are labeled in Fig. 3 as 0 and 1, i.e. the fundamental and 1st harmonic. Fig. 7 is a comparison of the modulations obtained. The strength or modulation of these components indicate the contrast, edge sharpness, and degree of periodicity in the field patterns. It is obvious that bands 5 and 7 are superior, implying that better discrimination between fields could be made with these bands, than with bands 4 and 6.

[3]J. W. Goodman, *Introduction to Fourier Optics*, New York, McGraw-Hill, 1968, Chapter 5.

Section 3

STATUS OF MICRODENSITOMETER ANALYSIS

Data Acquisition and Analysis

The status of required data received by us is as follows. A check indicates the data has been received.

		Aircraft (A/C)			ERTS-1
Set	Flight Date	Vinten	Scanner	#frames	MSS
1	8/22/72, 8/23/72 (Arizona)	✓	NA	184	✓
2	11/29/72 (San Francisco)	✓	✓*	18	✓
3	1/4/73 (San Francisco)	✓**	on order	51	on order
	4 and 5 scheduled for 3/73 - 5/73				

* Scanner data not suitable for analysis because of severe geometric distortion arising from the lack of a gyrostabilized platform on the A/C.

**Band 001 (green) malfunction, no imagery.

Noting that the data set 1 is not simultaneous, but taken 24 hours apart, we have given first priority to analysis of data set 2.

Because of cloud cover, the number of A/C frames from data set 2 was only 18. The frame over the northern end of Monterey Bay was selected for analysis because of the high spatial frequency content of the coast line. Fig. 8 shows the ERTS frame from 11/29/72. The line shown between points 1 and 2 was determined to be best for initial microdensitometer scanning because the points 1 (hill top) and 2 (corner of field), could be located reasonably easily in all bands of

the A/C and ERTS images. Using this line as a reference, several scans of the A/C and ERTS images are being made. These microdensitometer data will then be analyzed digitally to evaluate the OTF (Optical Transfer Function) for the ERTS system.

Because of severe geometrical distortion in the A/C scanner data from data set 2, we are restricted to using the Vinten camera imagery. Since the Vinten cameras are filtered to match the three bands of the ERTS RBV's, a comparison of the Vinten bands with the ERTS MSS bands is of interest. Fig. 9 is a plot of band sensitivities for all the sensors. The MSS data was supplied by Santa Barbara Research Center, the Vinten data on film and filters supplied by Ames Research Center, and the RBV data was redrawn from the ERTS Users Manual. Bands 4 and 6 of the MSS are approximated reasonably well by two Vinten bands, but band 5 is not so well matched. It should be kept in mind, when evaluating OTF data which we will obtain, that these bands are not identically matched. It is hoped that future A/C scanner data will be of better quality than that of data set 2, allowing good matching of spectral bands in both A/C and ERTS sensors.

For reference, the film•filter combinations for the Vinten cameras are listed below.

A/C Vinten Multispectral Sensor

A/C sensor ID	001	002	003
film	2402	2402	2424
filters	GG-475	OG-570	RG-645
	+	+	+
	BG-18	BG-38	9830

All cameras are 70 mm Vintens with 1.75 inch focal length lenses

Scan Lines

Fig. 10 is microdensitometer scans of the spikes in the Fourier spectra, caused by the periodic lines along the scan direction. For this image, it appears that the scan lines are weakest in band 6. Fig. 11 is reproduced from the Type I, Progress Report 2 for this contract, and shows the lines in one band of image #1104-17393. At the time of that report the cause of the lines was not known, but it was recently learned to be the result of calibration difficulties with one detector in each band. Noting the proximity of the fundamental frequency of the scan lines to the 1st harmonic of the agricultural fields (Fig. 3) it is conceivable that the scan lines could have a serious effect on estimation of field size, type, etc. if the orientation and scale of the fields in the image coincided with the 6-detector scan interval.

Edge Scans

Fig. 12 is reproduced from the Type I, Progress Report 2 for this contract, and shows microdensitometer scans of coast lines in image #1104-17393. Further analysis of these scans was abandoned when it was discovered that this image was one of several we received, which appeared to be exposed through the base of the film (see Progress Report 2). However, they remain valid as a relative comparison of edge variation from band to band.

Future Plans

The first digital microdensitometer data will be received shortly and we will proceed with calculation of the OTF for the ERTS MSS in bands 4, 5, and 6. With the five sets of A/C and ERTS data listed above we will not only obtain a valid estimate of the ERTS OTF but will hopefully be able to detect any changes in the OTF over a ten month period.

Acknowledgements

Mead Technology Laboratories (Dayton. Ohio), who have recently become an Industrial Associate of the Optical Sciences Center, are performing the microdensitometer scanning for this contract. They are cooperating fully with us to assure high quality data acquisition.

Frames Studied

#1129-18181

#1031-17325

Data Requests Submitted

1) dated about 1/15/73

2) dated 3/8/73

REPORT SUMMARY

Evaluation of ERTS-1 Image Sensor Spatial Resolution in Photographic Form

Type II Report #3

Category 9a - Sensor Technology

This report describes progress to date on contract number NAS5-21849 entitled "Evaluation of ERTS-1 Image Sensor Resolution in Photographic Form". The work described was carried out during the first six months of the contract from 1 September 1972 to 1 March 1973.

In the first part of this report we describe an analysis of the multispectral scanner (MSS) imagery in which a coherent optical system was used to display the spatial frequency content of the amplitude image.

The second part of this report deals with work preliminary to the microdensitometric scanning of near-simultaneous MSS and high altitude aircraft (A/C) imagery for the determination of the Optical Transfer Function (OTF) of the MSS for its four bands. The status of the data acquisition and analysis is described and some restrictions we have encountered are mentioned. The basic theory for this analysis procedure has recently been presented at the IX Congress of the International Commission for Optics in a paper entitled "Determination of the Inflight OTF of Orbital Earth Resources Sensors". A copy of this paper is included as an appendix to this report.

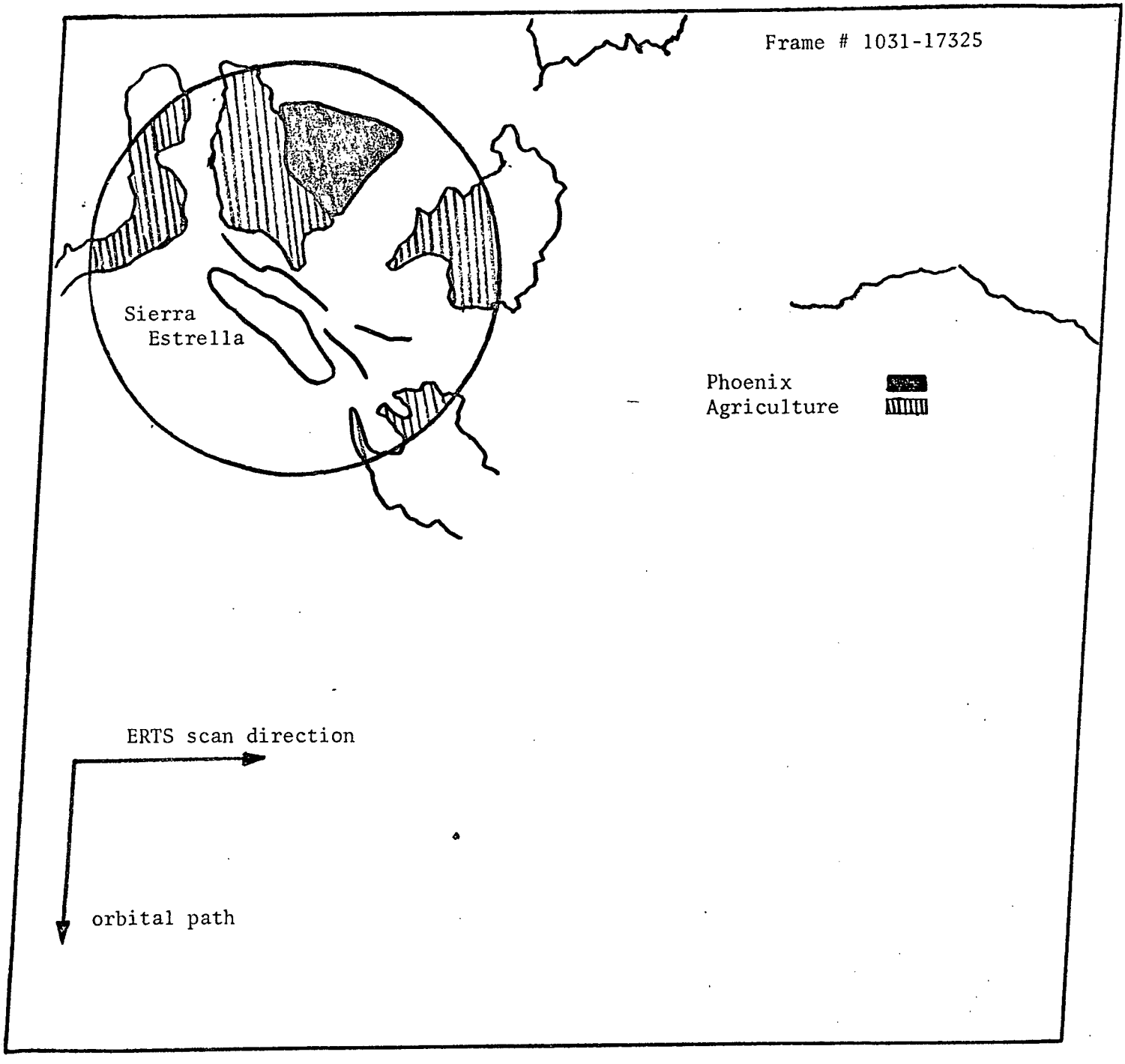

FIGURE 1

Diagram of ERTS frame used in optical Fourier analysis experiment. The circled area was Fourier transformed.

Apollo 9

Band BB

Band DD

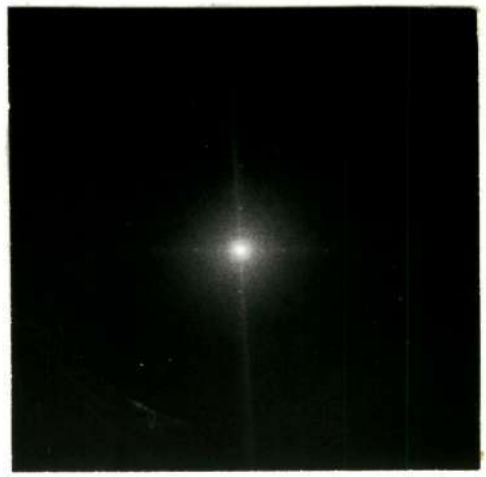

ERTS-1

Band 4

Band 5

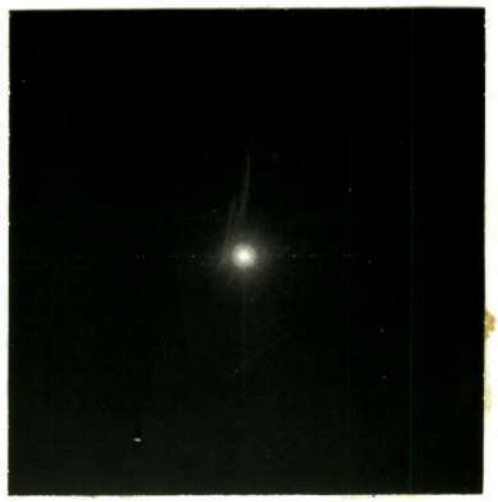

Band 6

Band 7

FIGURE 2

Prints of the Fourier spectra obtained from the Apollo 9 S065 experiment and ERTS images.

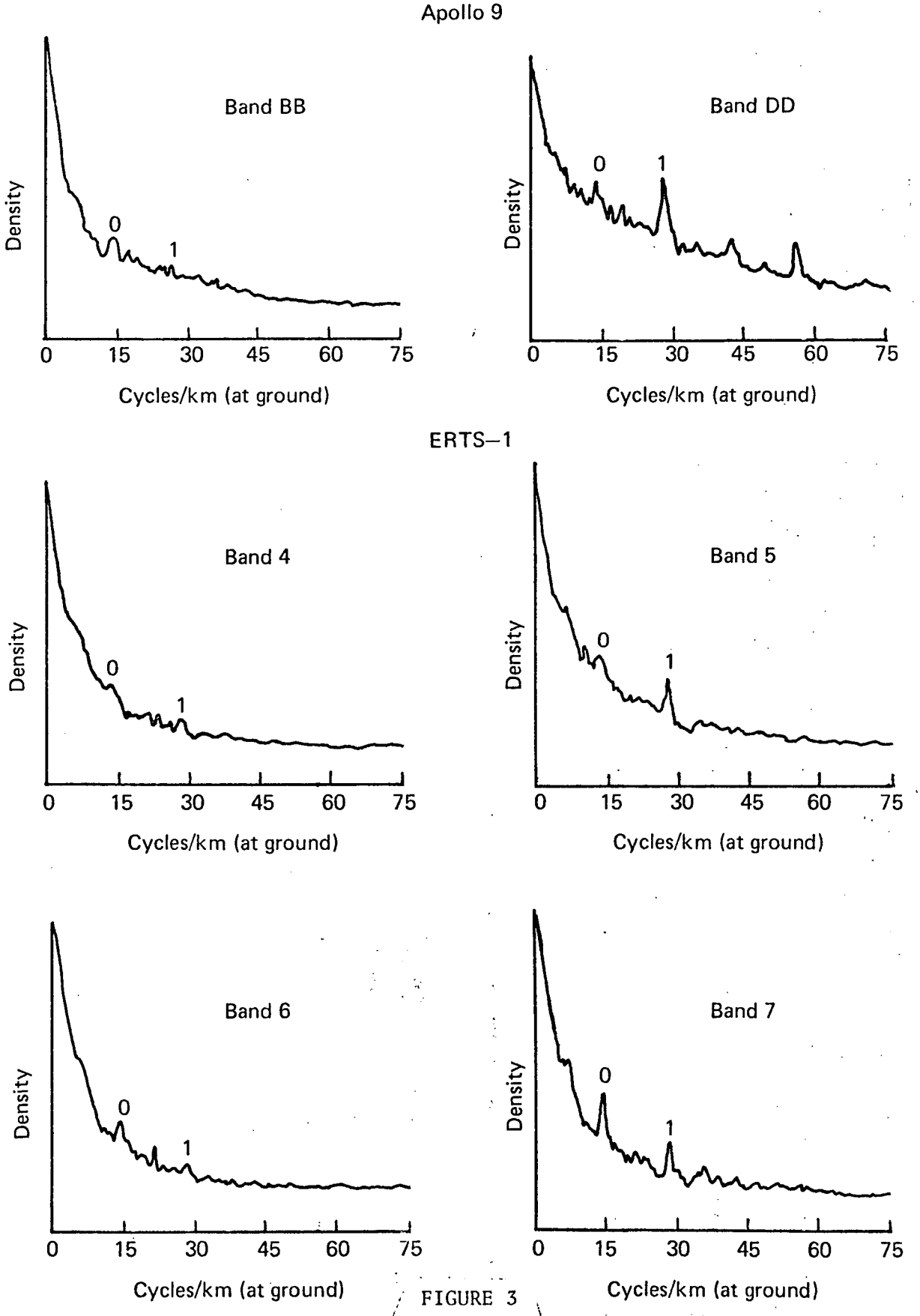

FIGURE 3

Microdensitometer scans along a selected azimuth of the photographically recorded Fourier spectra.

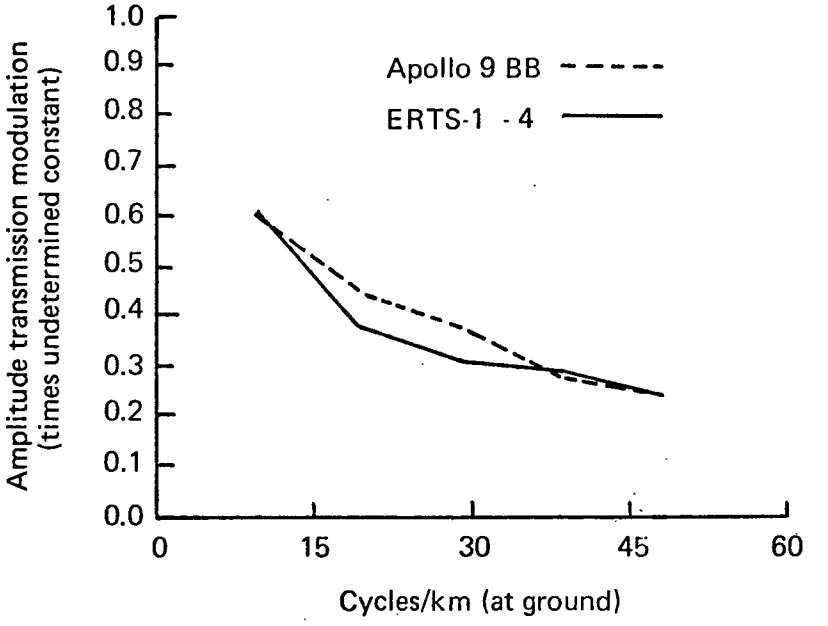

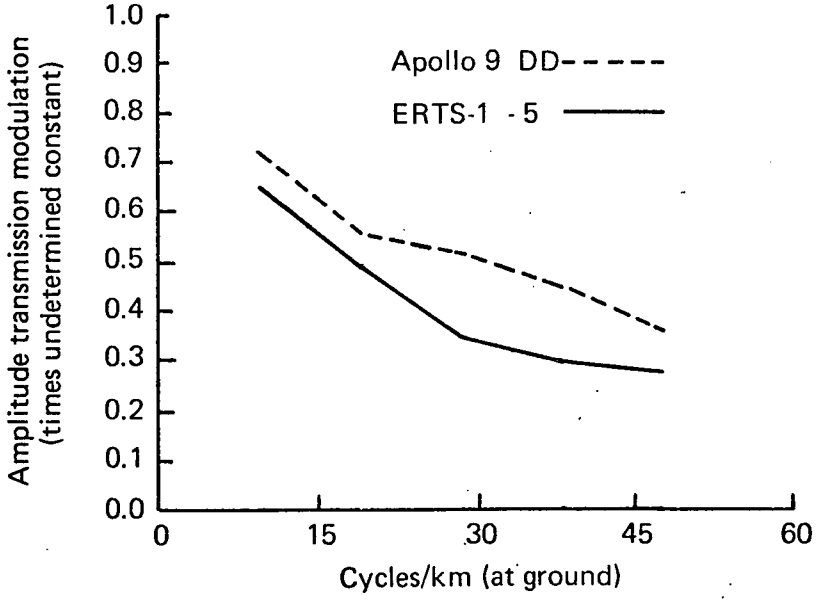

FIGURE 4

Amplitude transmission Fourier spectra.

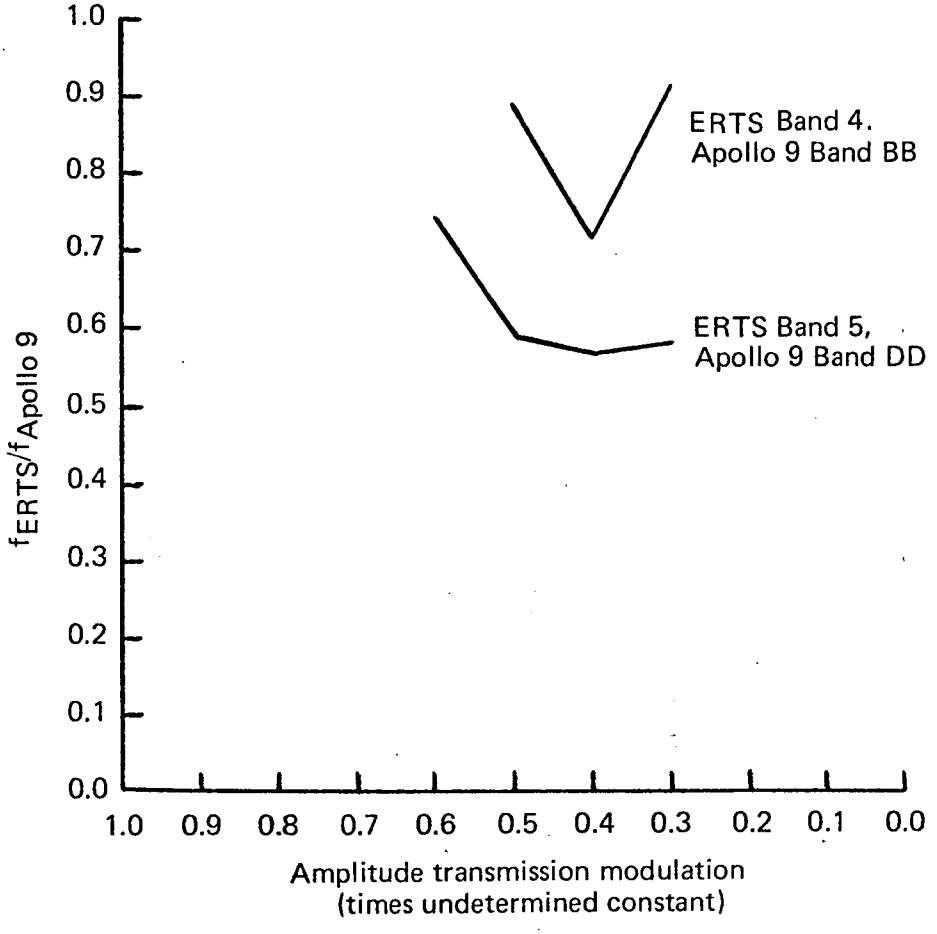

FIGURE 5

Ratio of spatial frequencies which have the same modulation in the ERTS and Apollo 9 S065 experiment images.

FIGURE 6
Amplitude transmission Fourier spectra.

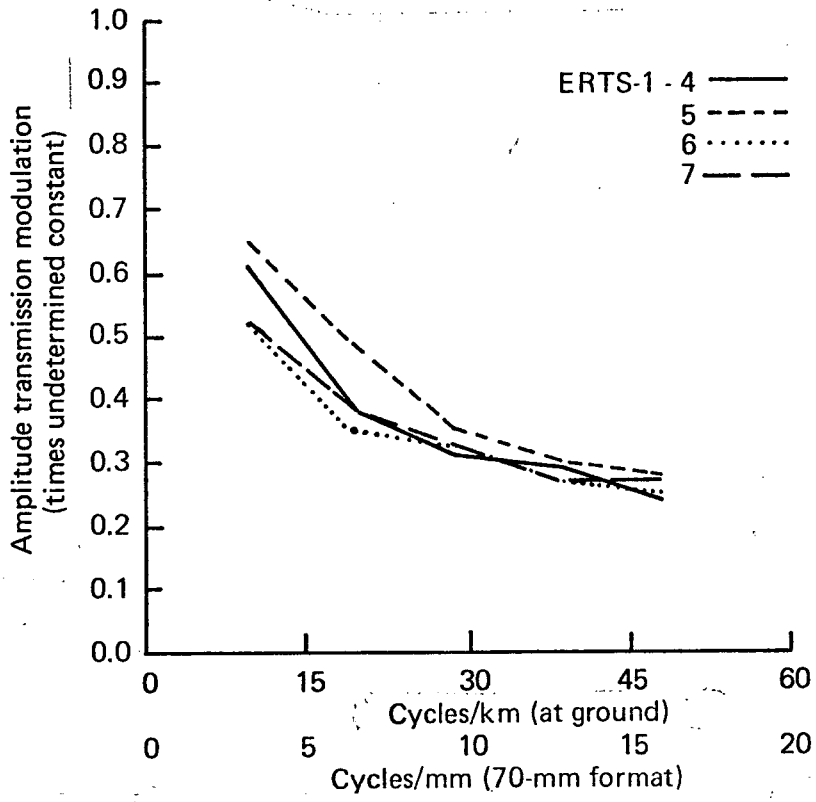

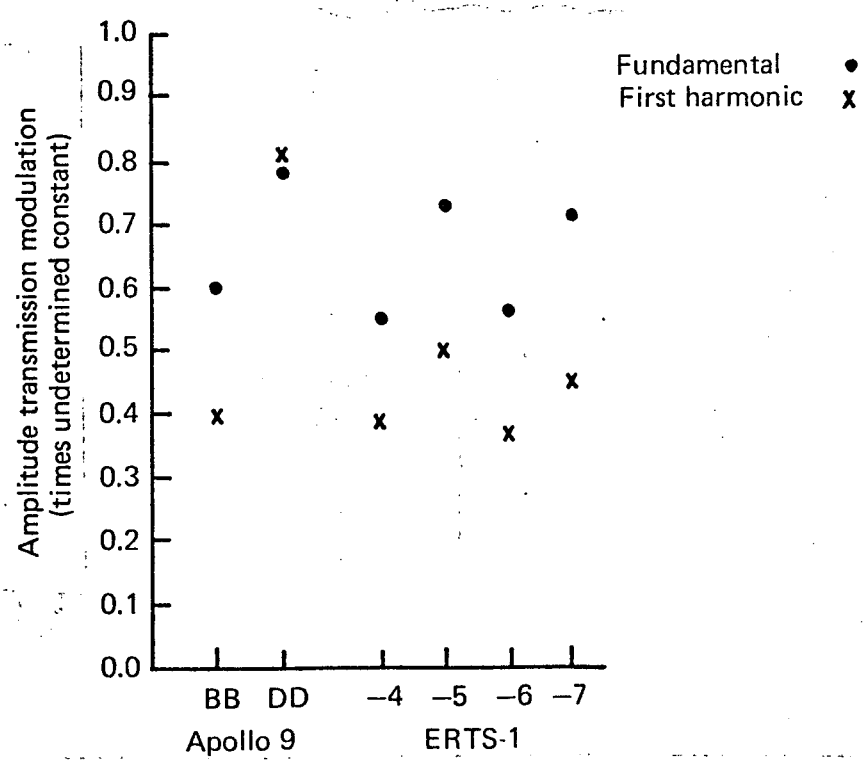

FIGURE 7
Modulation at two selected spatial frequencies in the ERTS and Apollo 9 S065 experiment images.

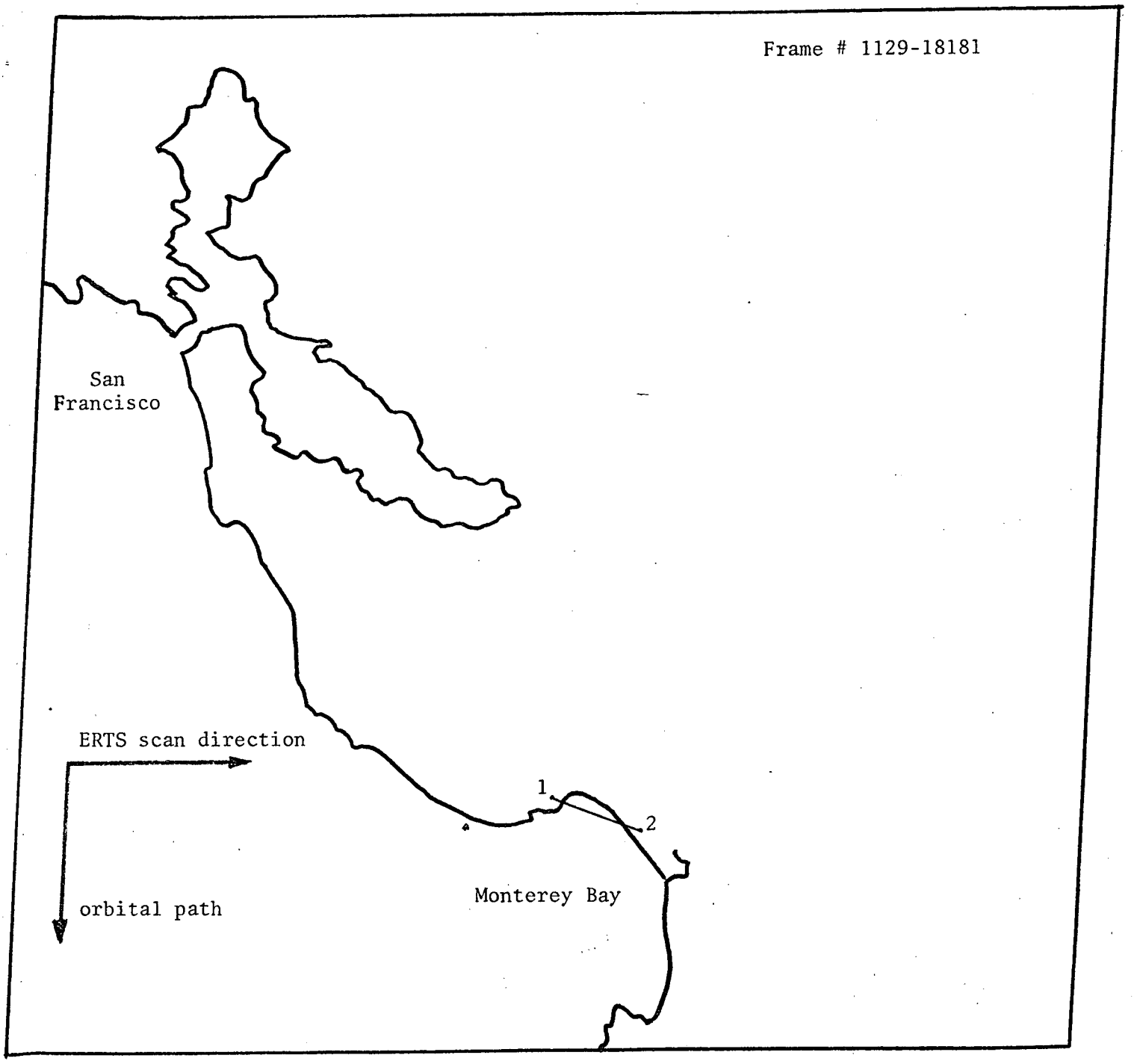

FIGURE 8

Diagram of ERTS image selected for microdensitometer analysis.

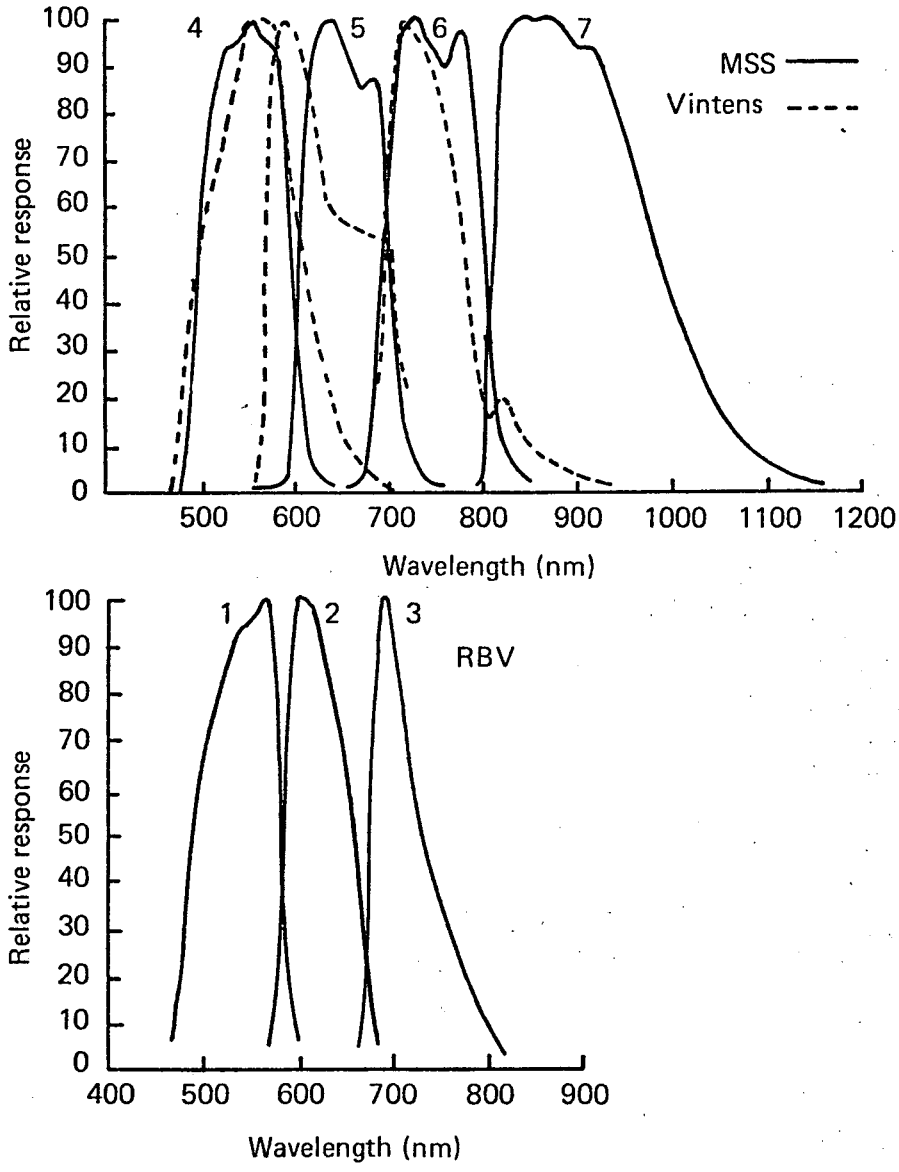

FIGURE 9

Spectral sensitivities of ERTS and U-2 aircraft multispectral sensors.

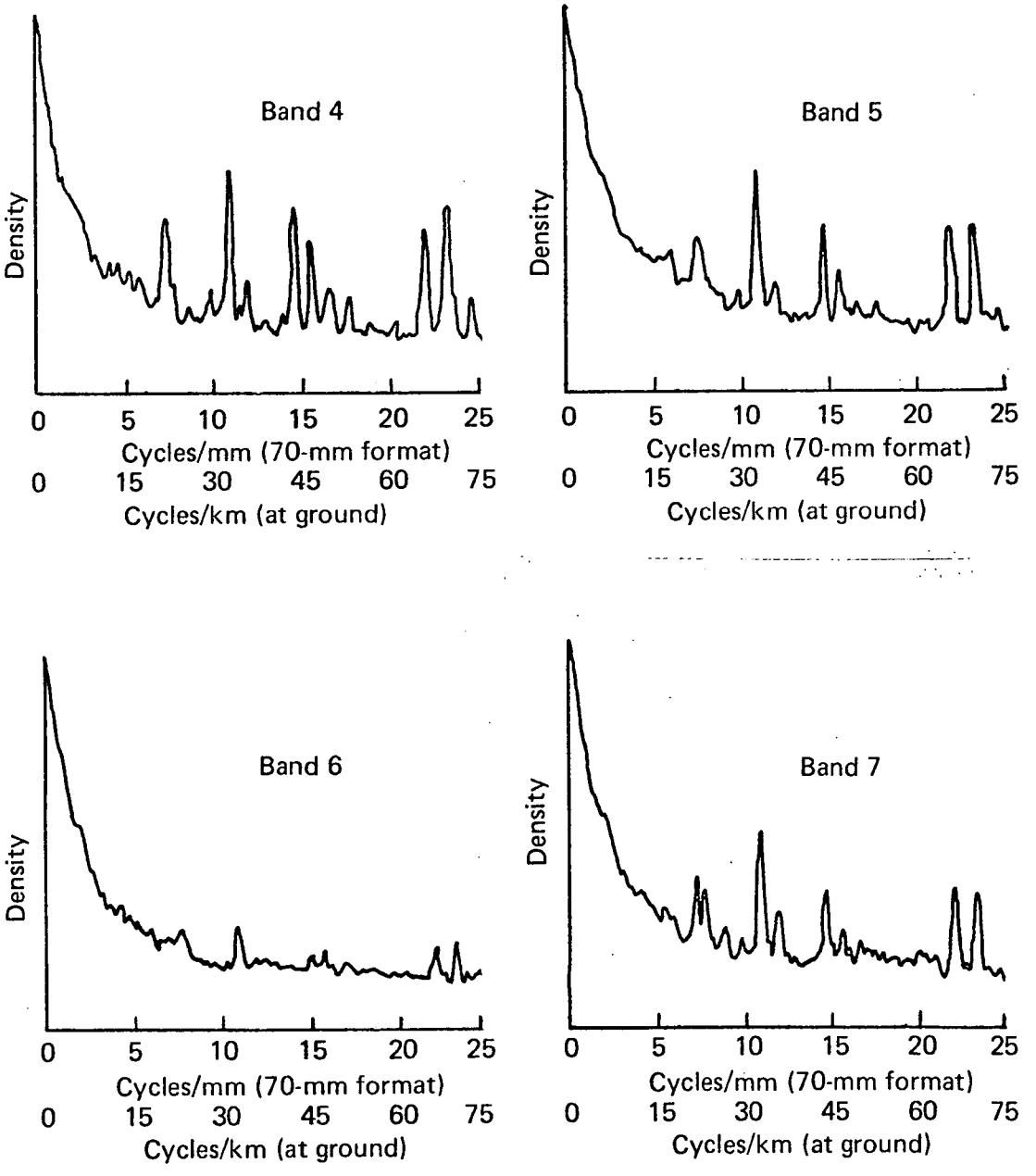

FIGURE 10

Microdensitometer scans of photographically recorded Fourier spectra, indicating effects attributed to the ERTS scan lines.

FIGURE 11

Microdensitometer scans of ERTS image #1104-17393.

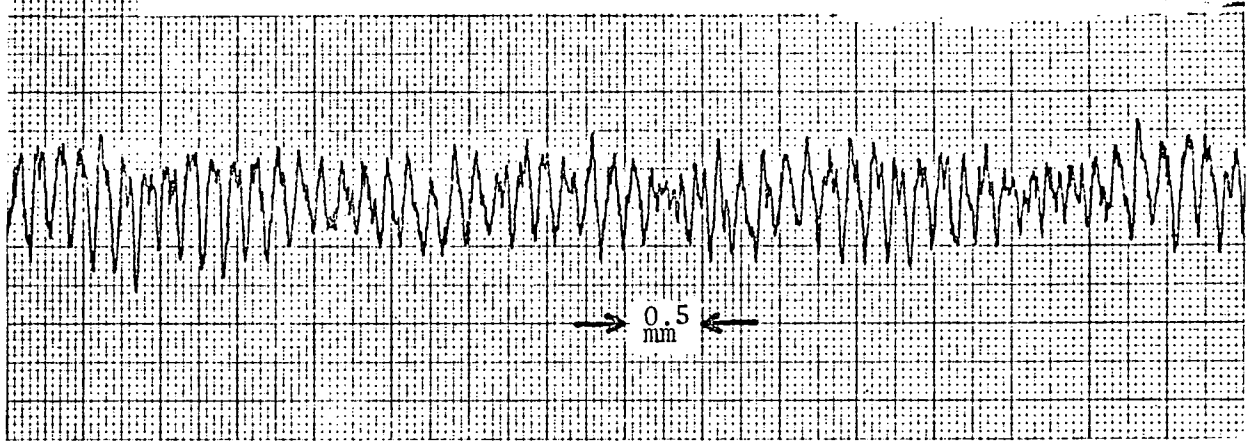

(a) Microdensitometer scan perpendicular to ERTS scan direction

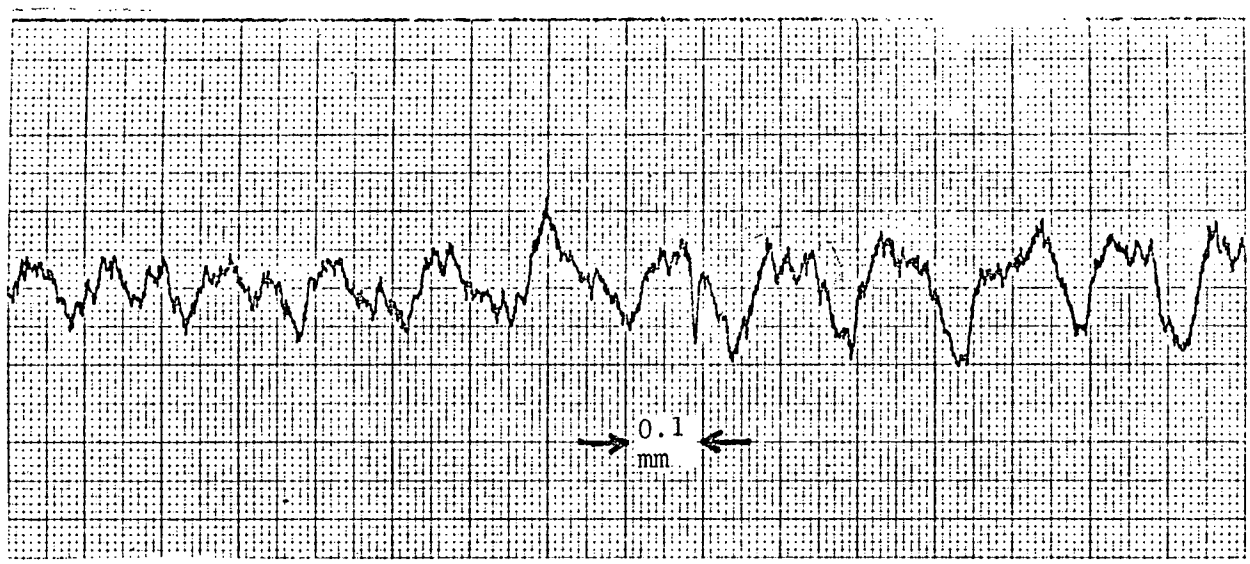

(b) Same as (a) with expanded horizontal (position) scale

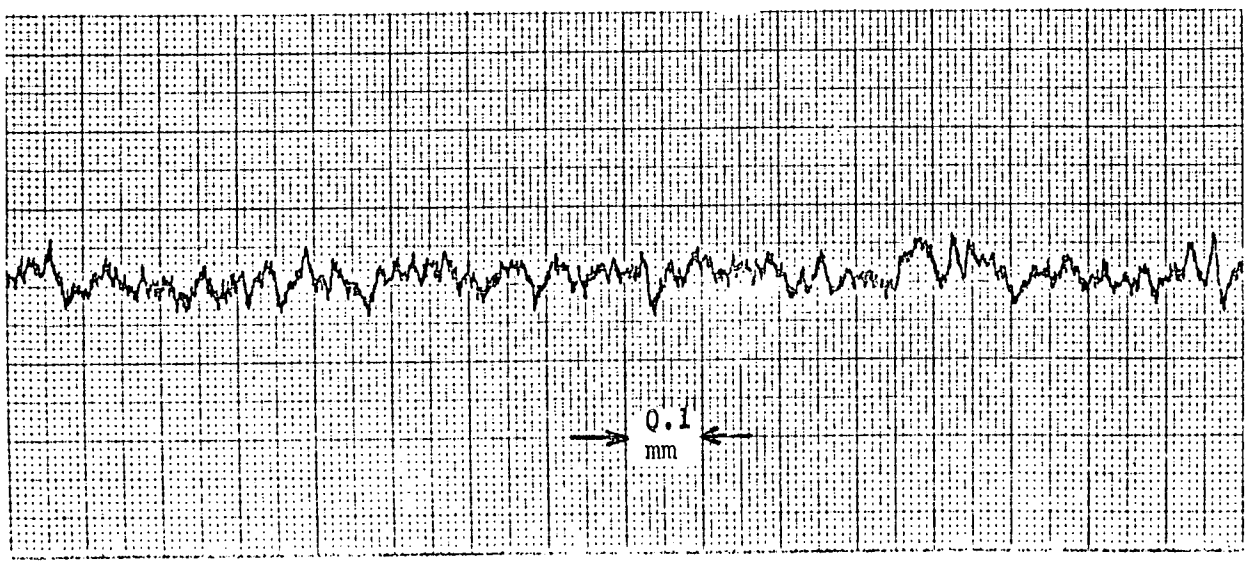

(c) Microdensitometer scan parallel to ERTS scan direction

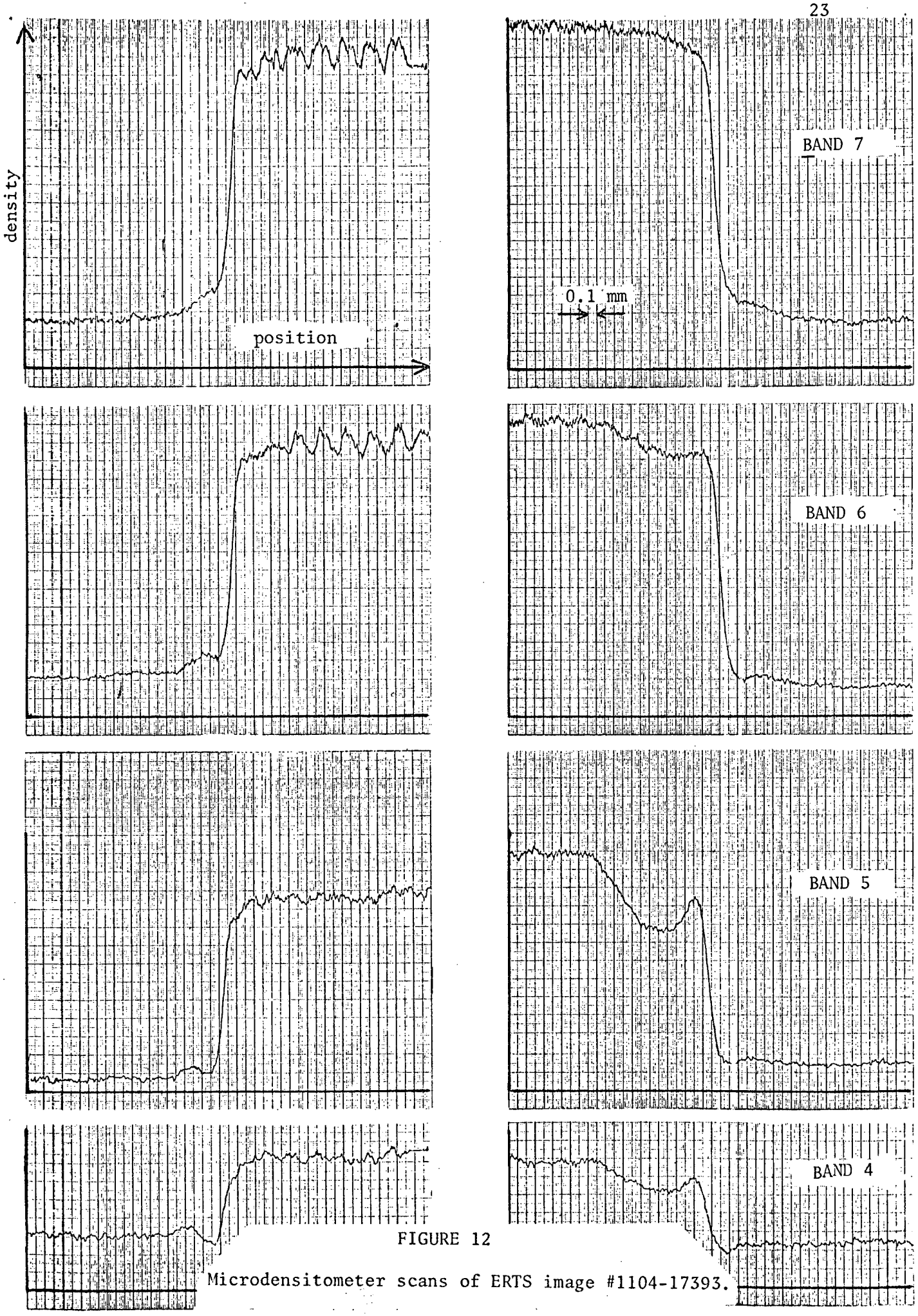

FIGURE 12

Microdensitometer scans of ERTS image #1104-17393.

EDGE 1

EDGE 2

APPENDIX

Determination of the Inflight OTF of Orbital Earth Resources Sensors

DETERMINATION OF THE INFLIGHT OTF OF ORBITAL EARTH RESOURCES SENSORS

Presented at the

IX Congress of the
International Commission for Optics
Santa Monica, California

October, 1972

by

R. A. Schowengerdt
P. N. Slater

Optical Sciences Center
University of Arizona
Tucson, Arizona 85721

ABSTRACT

The technique most widely used for detailed image evaluation of aerial and space photography has been edge analysis. Edges have been used because they appear more frequently in aerial scenes than do other simple objects such as points or lines. Methods for measurement and analysis of edges have been investigated extensively.

One fundamental limitation of analysis employing naturally occurring edges is that the object must be assumed perfect; i.e., the edge appearing in the scene is assumed to be exactly a step function, uniform on both sides and with a perfect discontinuity at the edge. This is certainly not true of natural edges such as coast lines, field boundaries, etc., and it is not generally true of randomly occurring man-made edges, for example building roofs, pavement boundaries, etc. Even if there is a perfect edge object in the scene, its position and orientation are unique, and hence the analysis is limited. In addition, for sensors with low ground resolution, such as those on the Earth Resources Technology Satellite (ERTS), the size requirements on man-made edges are prohibitive.

For these reasons we have investigated a technique that is largely independent of object scene. The approach is particularly applicable to evaluation of earth-orbiting multispectral sensors. In all programs employing such sensors, simultaneous underflight photography from aircraft is made during passes of the spacecraft.

To evaluate the spacecraft imagery, the two sets of photographs are scanned and digitized with a microdensitometer, the same ground area being scanned in each case. The data are then Fourier analyzed, and the spatial frequency spectra is calculated. The spatial frequencies in the underflight

trace are scaled to those in the spacecraft trace (by the ratio of altitudes if the two systems are of equal focal length), and the ratio of the spectra gives the in-flight OTF, $\tau(f)$, for the orbiting sensor,

$$\tau(f) = I(f)/O(f)$$

In detail we must calibrate the spectroradiometric and distortion characteristics of the underflight sensor in the region of the image field that was scanned with the microdensitometer. Furthermore, the transfer function of this system must be known for the same region. However, because of the scale change for comparison of the images, we are interested only in very low spatial frequencies in the underflight image, thus relaxing the requirement on exact knowledge of the underflight sensor OTF.

The method has been applied to an Apollo 9 (S065 experiment) frame, and the sensor OTF has been calculated. Image quality was also compared, using the same method, in second and fourth generation copies of the original film. The results are good enough to encourage use of the technique and to indicate the accuracies required of the various measurements involved in determining in-flight sensor OTF by this method.

Results of investigations in progress will be presented. A technique for determining correct scan registration and scaling between the two sets of imagery will be dissussed and a promising approach to noise reduction, in the form of weighted averaging of OTF's from several scans, will be described.

I. INTRODUCTION

The past few years have seen an increasing interest in the worldwide assessment of natural resources and the detection of environmental pollution. A common characteristic of many instruments used for such purposes is that they monitor radiation reflected from, or emitted by large areas of the earth's surface, in different parts of the electromagnetic spectrum. Frequently, the output from these instruments, which are referred to as multispectral remote sensors, is converted into a photographic image for analysis purposes. For example, the density function of the image may be digitized with a microdensitometer. The resulting values are related to ground reflectances (not a straightforward task), which are used as an aid in the production of thematic maps from the imagery.[1]

One subject of practical interest to those analyzing imagery from orbiting spacecraft is the quality of the imagery, which is expressed in terms of spatial resolution and spectroradiometric accuracy, quantities that are related and equally important in remote sensor imagery. The blurring of the object, which occurs in any image, decreases the accuracy of spectroradiometric calculations on microimage areas, particularly when the image modulation is decreased to the point where it becomes indistinguishable from noise.

We are concerned here with techniques for measuring the quality of operational imagery and in particular with a method that is uniquely suited to the characteristics of orbiting multispectral sensors. In the next section several of these characteristics will be discussed from the viewpoint of their importance to the image evaluation problem.

Factors Influencing the Selection of an Image Evaluation Method

In selecting an inflight image evaluation method we first have to take into account the unique characteristics of both orbital multispectral sensors and the imagery they produce. Multispectral sensors form several images of the ground scene simultaneously through broad band spectral filters or dispersive elements. Now in general the spatial distribution of scene radiance will be different from band to band. Thus, the edge between two fields may be a good step function in a red band, but owing to sparse vegetation near the edge, it may be a poor step function in a green band. Consequently a given object, particularly a naturally occurring one, may not be suitable for evaluating the image in all bands of the sensor. In addition, wavelength-dependent scattering of light in the atmosphere will reduce the modulation of the image by different amounts in each band. The signal-to-noise ratio will therefore vary from band to band even if the image recording components in each band are identical. Moreover, the optical system(s) used in the sensor will generally have different imaging characteristics in each band because of the dependence of aberrations on wavelength.

The low ground resolution typical of these sensors bears directly on the choice of an image evaluation method. Table 1 below compares the resolution of low-contrast, three-bar ground targets for past, current, and future systems:[2,3]

Table 1

Resolution of Earth-Orbiting Remote Sensors

Sensor	Approximate Ground Resolution m/line pair	line pair/km
Apollo 9 S065 experiment (4 Hasselblad cameras)	100	10
ERTS-1 (Earth Resources Technology Satellite)		
RBV (Return Beam Vidicon)	180-280	3.5-5.5
MSS (Multispectral Scanner)	300	3.5
Skylab S190 experiment (6-lens Itek camera)	20-100	10-50

As we will discuss further in the next section, these values generally rule out the possibility of utilizing man-made test targets.

Finally, in all earth remote sensing programs involving spaceborne sensors, for example, those onboard NASA's Earth Resources Technology Satellite, simultaneous underflight photography is scheduled regularly. The imagery from these underflights is used as an aid for calibration of spacecraft data in terms of ground measurements. The aircraft sensors usually use the same spectral bands as those in the spacecraft and in some cases duplicate systems are under construction.[4] Simultaneous underflights are flown from low altitudes of a few hundred meters to very high altitudes of 15 to 20 km. The imagery from these underflights is necessary for the image evaluation technique discussed in this paper.

Review of Current In-Flight Image Evaluation Techniques

Sensor imaging capabilities can be predicted at the design stage and measured in the laboratory for complete systems. However, sensor performance cannot be predicted accurately and reliably for an extended operational period in the space environment. Imaging systems carried by aircraft are often evaluated in-flight by the use of the three-bar resolution type of ground target. In this discussion we are concerned, however, with a more complete analysis that extends to the measurement of the optical transfer function (OTF), which is symbolized by $\tau(\bar{f})$ where $\bar{f}$ is a (possibly) two-dimensional spatial frequency variable.

Measurement of $\tau(\bar{f})$ for in-flight sensors has been achieved with the use of special objects such as man-made edges[5] or lines[6] and their naturally occurring counterparts in the form of coast lines, field boundaries, lunar crater edges,[7] etc. The use of naturally occurring targets has several limitations. Ideal edges and lines do not occur in nature and reasonable facsimiles are often of unknown quality. As mentioned earlier, a given target may not be suitable for the evaluation of all the bands in a multispectral sensor. Furthermore, the low ground resolution typical of many of these sensors sets a severe requirement on the minimum size of both natural and man-made targets. Consider a sensor with a 100-m/cycle ground resolution and let that distance correspond roughly to the half width of the central lobe in the sensor spread function. Then, if we want to measure the first or second side lobes of the spread function, the length of

the target in any given direction must be at least 200 to 300 m and at least that long in the perpendicular direction. Naturally occurring objects that are large and straight over that length would be difficult to find, and deployment and maintenance of such large man-made targets would be difficult if not impossible. Even if such an object was used, its position and orientation in the field of view would be unique, and consequently its use would be limited.

The technique we will describe can be applied to any imagery for which there is simultaneous underflight coverage, and it does not have any direct dependence on the nature of the object. Consequently, it is of more practical value than an analysis using isolated targets.

II. THEORY

The fundamental imaging equation for linear, stationary optical systems is

$$I(\bar{f}) = \tau(\bar{f})O(\bar{f})$$

where $I(\bar{f})$ and $O(\bar{f})$ are the image and object spatial spectra, respectively. In general, all quantities in this equation are complex.

To measure $\tau(\bar{f})$ it is necessary to know $I(\bar{f})$ and $O(\bar{f})$. As discussed above, $O(\bar{f})$ is not known for naturally occurring objects. Man-made targets are often used because $O(\bar{f})$ is then known and $I(\bar{f})$ can be measured from the imagery. Now the simultaneous underflight imagery obtained in multispectral sensor experiments gives us a good measure of $O(\bar{f})$ for any part of a scene. The scale factor between the underflight imagery and the spacecraft imagery indicates that we need measure only very low spatial frequencies in the underflight image and then scale these up to the correspondingly higher frequencies in the spacecraft image to evaluate $\tau(\bar{f})$. For example, if the cutoff frequency (assuming noiseless imagery) of the spacecraft sensor OTF is 50 cycles/mm and the aircraft underflight sensor is of the same focal length and flown at an altitude 1/10th of that of the spacecraft, frequencies up to only 5 cycles/mm need to be measured in the underflight image. To determine $O(\bar{f})$, the OTF for the aircraft sensor should be divided into the underflight image spectrum, but the highest frequency of interest, which in the above case is 5 cycles/mm, may be so low that this correction is unnecessary.

In practice, the two sets of images from the spacecraft and the simultaneous underflight can be scanned and digitized with a microdensitometer in either one or two dimensions. The same ground area is scanned in each set of images, and the scanning aperture size and sampling rate are scaled by approximately the scale between the images. Because of the scale factor, the aperture size is large for the underflight image. In the previous example, the aperture size would be about 100 to 200 μm. Photographic grain noise is thus a minor problem in the measurement of $O(\bar{f})$. For one-dimensional scans a slit aperture can be used to reduce the grain noise even further.

Now, the spacecraft image scan should not be longer than the size of an isoplanatic, or stationary, region to ensure that $\tau(\bar{f})$ is essentially constant over the scan length. Because the same ground area is scanned in each of the two images, the length of the underflight image scan is longer than the spacecraft image scan. Thus, the underflight image scan may extend over a significant part of the field (say 5° to 10°) and care should be taken that this scan also does not extend outside an isoplanatic region. However, the restriction to low frequencies in this image means that the underflight sensor OTF, in this frequency range, will likely be constant over the scan length.

In addition to the sensitometric conversion from film density to effective image irradiance for all data, the underflight image data should be corrected for $\cos^4$ falloff in irradiance off axis.

Distortion in the underflight image owing to topographic elevation differences on the ground should be considered. The

positional distortion Δr for an image point at a distance r from the center of the image is given by

$$\Delta r = r \frac{\Delta H}{H}$$

where ΔH is the difference in ground elevation of the on-axis object point and the point imaged at r, and H is the aircraft altitude. For H = 20 km, ΔH = 100 m, and r = 10 mm, we have Δr = 0.05 mm, which is less than the required microdensitometer aperture size mentioned earlier and would be considered negligible. For each scan, however, it would be prudent to check topographic maps of the area, estimate the distortion from elevation differences, and, if necessary, apply a correctional transformation to the data.

Because it is unlikely that the aperture size and sample interval could be scaled exactly on the microdensitometer, correction for aperture and microdensitometer OTF and exact scaling of the data must be done on the digitized data in a computer. A technique for scaling that has been successful is to start at the same ground point in both the spacecraft and underflight image, take the same number of points in each set of data but with the sample interval on the underflight image chosen as close as possible to the scale factor times the sample interval on the spacecraft image, and stretch or shrink the underflight image in consecutive steps by a linear interpolation scheme, which keeps the number of points constant. The integrals

$$\text{mean squared difference} = \frac{\int [o(x) - i(x)]^2 dx}{\int [o(x)]^2 dx}$$

$$\text{correlation factor} = \frac{\int o(x)\, i(x)\, dx}{\int [o(x)]^2 dx}$$

are evaluated for each step of the stretching or shrinking process. A minimum will appear in the mean squared difference between object and image at some scale factor and a maximum will appear in the correlation factor, usually at the same scale factor. We thus have two independent criteria for determining the scale factor. In addition, by using this procedure, the same number of real points is obtained in each set of data, which allows us to use a fast Fourier transform (FFT) routine that performs two real transforms simultaneously, an efficient use of the FFT algorithm.

After correction for microdensitometer OTF, sensitometry, and scaling, the data are Fourier transformed, and the ratio of corresponding spectral values gives the OTF of the spacecraft sensor. Now, in any procedure that involves sampled data and calculation of spectra, the spectra are replicated in the frequency domain at intervals of $1/\Delta x$, the sample interval. If Δx is too large, overlap of the spectra may occur, which results in aliasing,[8] i.e., high frequencies appearing as lower frequencies. We would expect aliasing to be most severe in the underflight image data where large values of Δx are used. However, the microdensitometer aperture is also large and consequently serves to reduce the modulation of higher frequencies and thus also the aliasing. Using underflight data from the Apollo 9 S065 experiment we have determined the aliasing errors in Table 2 for *one particular* image spectrum.

The same set of data was used but was sampled at different intervals. The error was measured only for frequencies below the first zero, f_c, of the scanning aperture OTF.

Table 2

Aliasing Error

f_c	Δx (mm)	$1/\Delta x$ (cycles/mm)	Maximum aliasing error	
			Modulus	Phase
5 cycles/mm	0.012	83	assumed zero	assumed zero
	0.024	42	5%	10%
	0.048	21	5%	50%
	0.096	11	5%	50%

In this example, the phase errors occurred only in the region of 2.5 to 5 cycles/mm.

Finally, we note that the low ground resolution and the large final product format sizes (S065 - 70-mm, ERTS - 24-cm) typical of orbital multispectral images means that the requirements placed on microdensitometry by the above technique are not severe. For example, in evaluating the S065 system, aperture sizes of 0.02 by 0.1 mm and 0.2 by 1.0 mm and sample intervals of 0.006 mm and 0.06 mm were used on the spacecraft and underflight imagery, respectively.

III. EXAMPLES OF DATA FROM APOLLO 9 SO65 EVALUATION

Figure 1 shows microdensitometer scans of the image of the same ground area in each of three bands: BB (green filter, Pan-X film), CC (near-ir filter, black and white ir film), and DD (red filter, Pan-X film). The curves illustrate some of the statements made earlier. For example, the modulation in the BB band is the lowest of the three, which is due to atmospheric scattering and to low modulation of the object in the green band (the image was of southern Arizona). Also note that grain noise in the ir band is more prominent than in the other two bands owing to the high granularity of the ir film.

Figure 2 is a plot of the mean squared difference and correlation factor between the underflight (object, o) and spacecraft (image, i) scans (DD band) as a function of scale factor. It can be seen that a scale factor of about 10.7 gives the best match between object and image. The curves indicate that the two criteria for matching are sensitive to the scale factor, and it is expected that an accuracy of ±2.5% can be obtained in determination of the scale factor.

Figure 3 shows the image function (DD band) and the object function as originally sampled and at the correct scale factor. The same number of points is represented in each curve.

Figure 4 illustrates the effects of aliasing. The modulus and phase of the spectrum of a set of underflight data, sampled at two different intervals, are shown. At the greater sample interval, the modulus has a positive error increasing at higher frequencies, and the phase shows varying error, also increasing at higher frequencies.

Figure 5 is the OTF for the DD band, and represents the average of OTF's obtained from several portions of one scan. The real and imaginary spectral components of the OTF determined from each set of data were weighted by the strength of the image spectrum modulus and then averaged to obtain the final OTF. The dashed bounds on the lower section of the MTF represent relative uncertainty based on the strength of the image modulation at each frequency. Additional smoothing of the OTF was achieved by eliminating negative lobes in the corresponding spread function and by convolving the OTF with a gaussian function. The curves are dashed above 25 cycles/mm because they have not been corrected for aliasing in this region. The effect of aliasing is particularly evident in the phase transfer factor.

IV. DISCUSSION OF THE TECHNIQUE

One of the difficulties in using natural terrain for image evaluation as discussed in this paper is the low modulation of the ground as seen from above the atmosphere. The recorded images are of even lower modulation and the signal-to-noise ratio, i.e. (image modulation)^2/ grain noise variance, which is a function of spatial frequency, can easily be as low as 5:1 and decrease rapidly with increasing spatial frequency. With edge analysis, multiple scans are usually averaged to increase the signal-to-noise, but this is not possible with the general technique described here. However, it is possible to decrease the uncertainty in the OTF by averaging OTF's obtained from several scans within an isoplanatic region.

Locating exactly the same ground area and determining the scale between the two images are problems with this approach, but they can be handled satisfactorily by mean square difference and correlation matching.

In spite of these difficulties, our approach possesses several unique assets. The orbiting sensor OTF can be determined from any imagery (and in any portion of the field of view) that is covered by simultaneous underflights. There is no need for special targets or reliance on natural objects of unknown quality as test objects. Indeed, the use of natural terrain for image evaluation provides additional information about the usefulness of the imagery. Those analyzing remote sensing data can use the statistical results of visual or machine-aided photointerpretation to establish relationships among the quantity and quality of data extractable from the imagery, the spatial frequency content of the imagery, and the sensor OTF. These relationships would not only be useful for determining the value of given imagery, but also for specifying requirements on future sensors.[9]

The technique has been applied to evaluation of the Apollo 9 SO65 photography[10] and is currently being used at the Optical Sciences Center for quality evaluation of the ERTS-1 RBV and MSS sensors.

We wish to acknowledge NASA's continuing support of this effort under contract NAS 9-9333 for the Apollo 9 studies and contract NAS 5-21849 for the ERTS-1 investigation.

REFERENCES

1. A. B. Park, "Earth Resources Program," presented at the ICO-IX Congress on Space Optics, Santa Monica, California, Oct. 1972.
2. A. P. Colvocoresses, "Image Resolutions for ERTS, SKYLAB and GEMINI/APOLLO," Photogrammetric Eng. 38 (1): 33-35, Jan. 1972.
3. P. N. Slater, "Multiband Cameras," Photogrammetric Eng. 38 (6): 543-555, June, 1972.
4. R. E. Forkey and D. A. Womble, "Unique Lens Design for Multiband Cameras," presented at the ICO-IX Congress on Space Optics, Santa Monica, California, Oct. 1972.
5. P. G. Roetling, R. C. Haas, and R. E. Kinzly, "Some Practical Aspects of Measurement and Restoration of Motion-Degraded Images," *Evaluation of Motion-Degraded Images*, NASA SP-193, 1969.
6. L. O. Hendeberg and E. Welander, "Experimental Transfer Characteristics of Image Motion and Air Conditions in Aerial Photography," Appl. Opt. 2 (4): 379-386, April 1963.
7. M. J. Mazurowski and R. E. Kinzly, "The Precision of Edge Analysis Applied to the Evaluation of Motion-Degraded Images," *Evaluation of Motion-Degraded Images*, NASA SP-193, 1969.
8. R. B. Blackman and J. W. Tukey, *The Measurement of Power Spectra*, New York, Dover Press, 1959, p. 31.
9. P. N. Slater and R. A. Schowengerdt, "The Specification of Sensor Performance for Earth Resources Studies," Photogrammetric Eng., in press.
10. R. A. Schowengerdt and P. N. Slater, "Final Post-flight Calibration Report on Apollo 9 Multiband Photography Experiment S065," NASA contract NAS 9-9333, May 1972.

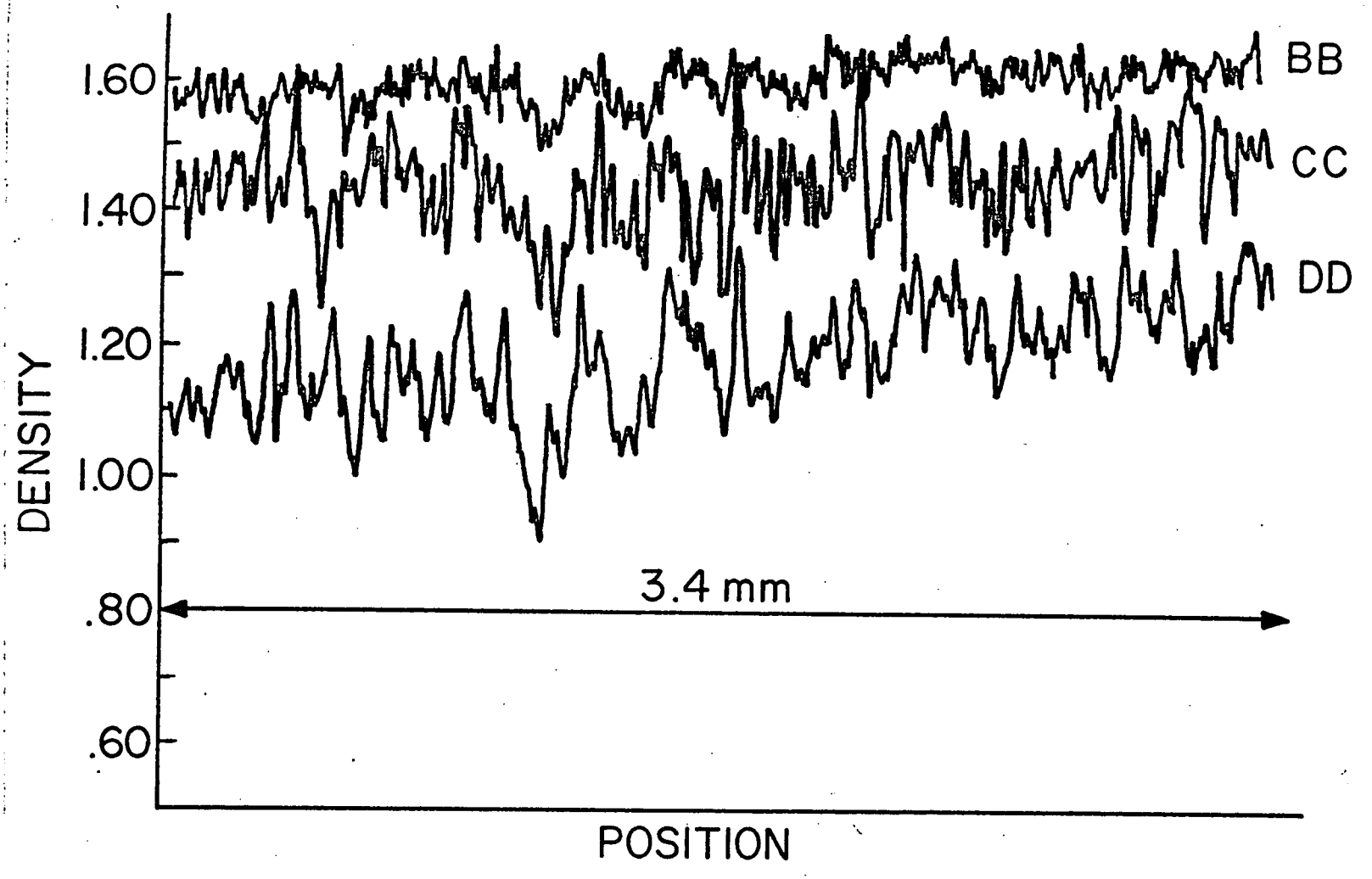

FIG. 1. IMAGE SCANS, SPACECRAFT IMAGERY.

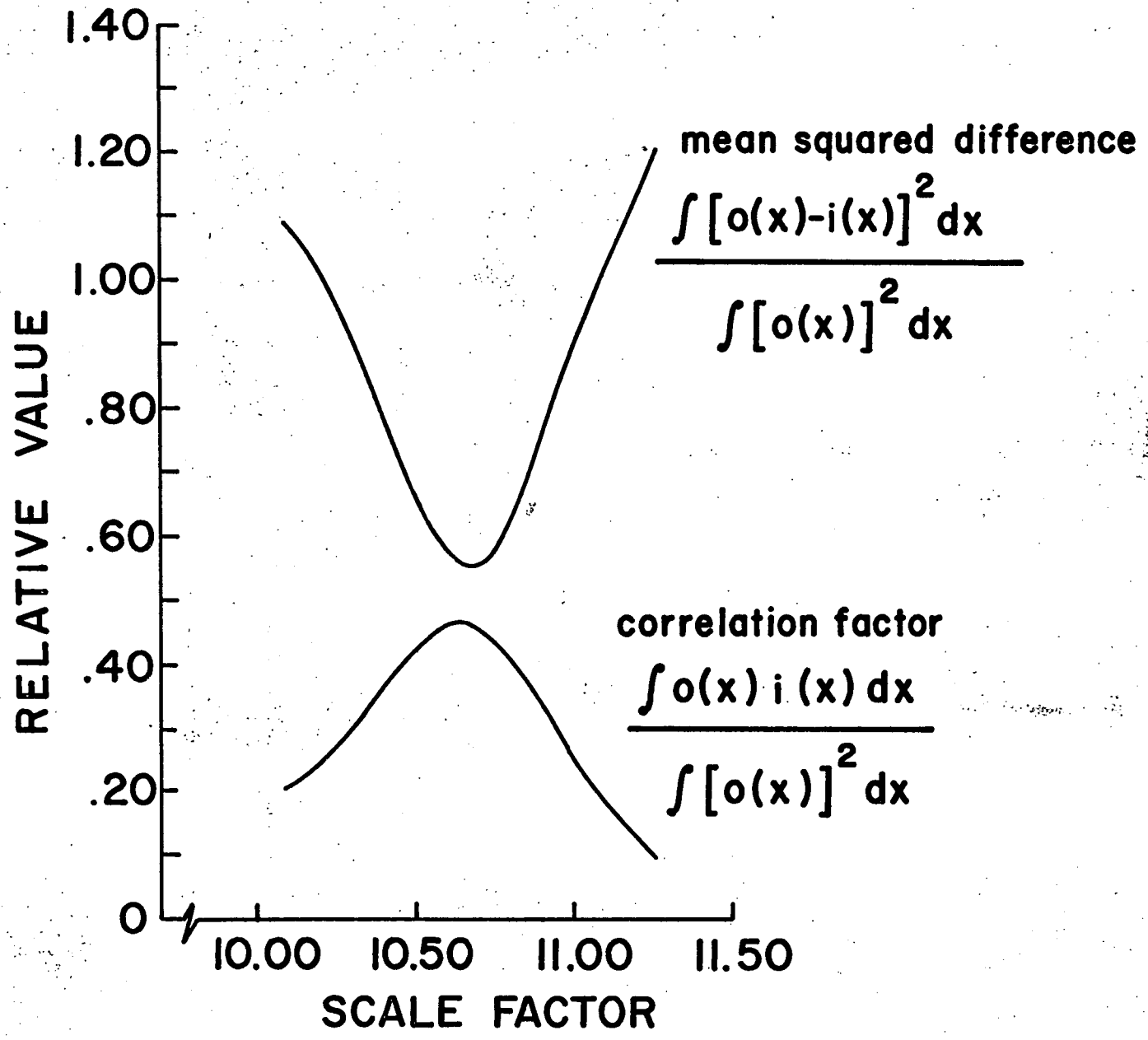

FIG. 2. CRITERIA FOR SCALE FACTOR DETERMINATION

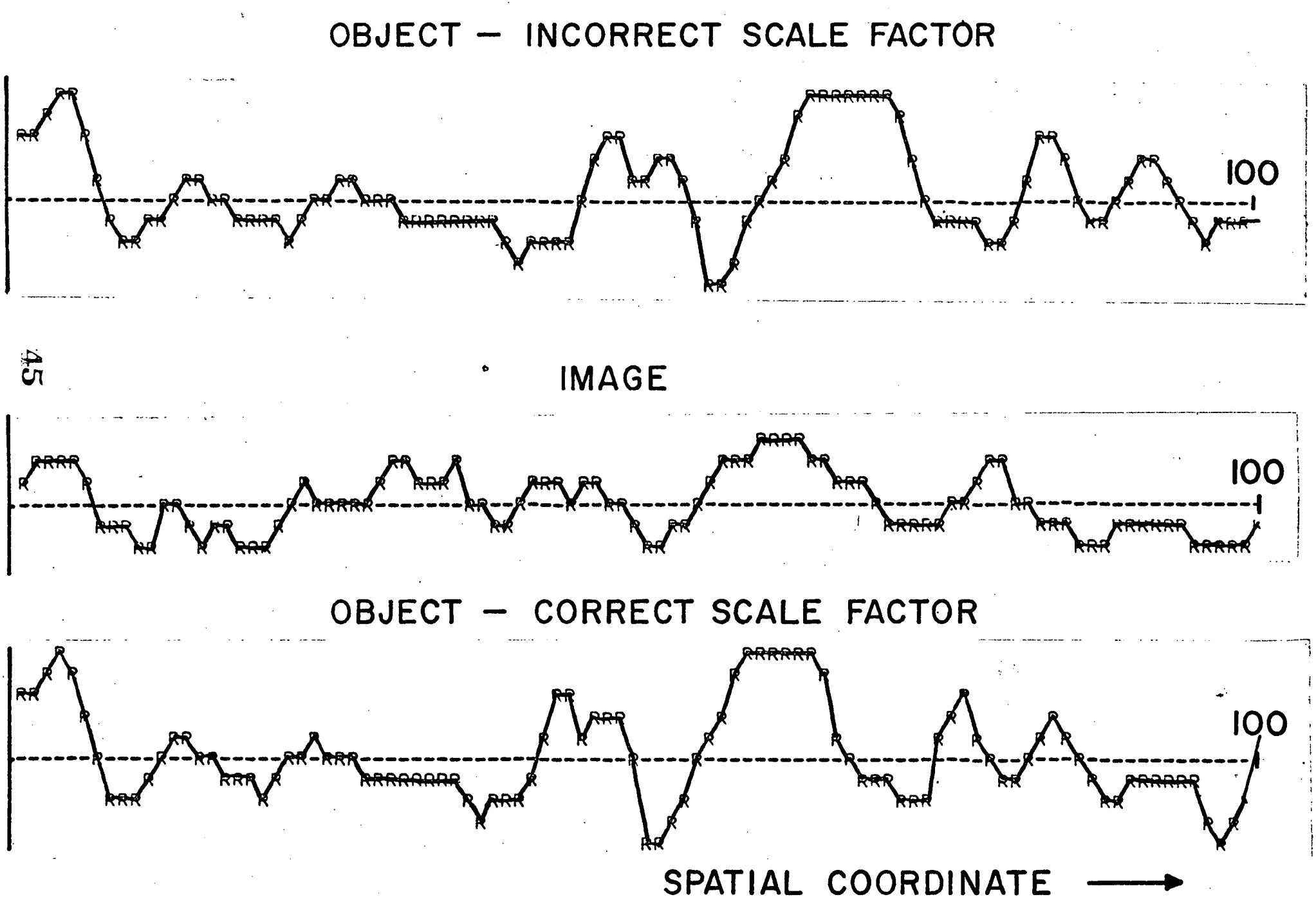

FIG.3. SCALING OF OBJECT TO IMAGE

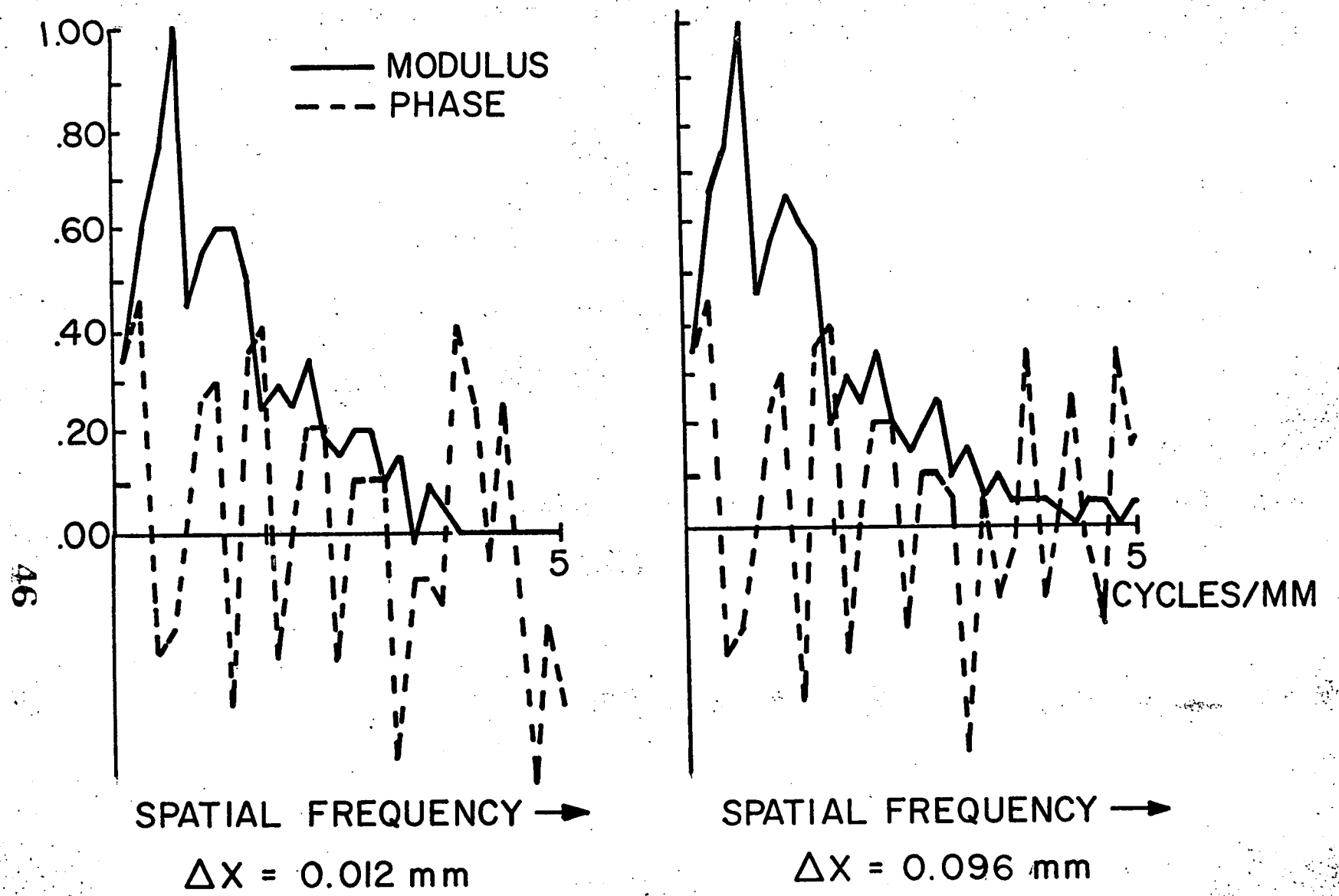

FIG. 4. ALIASING ERROR

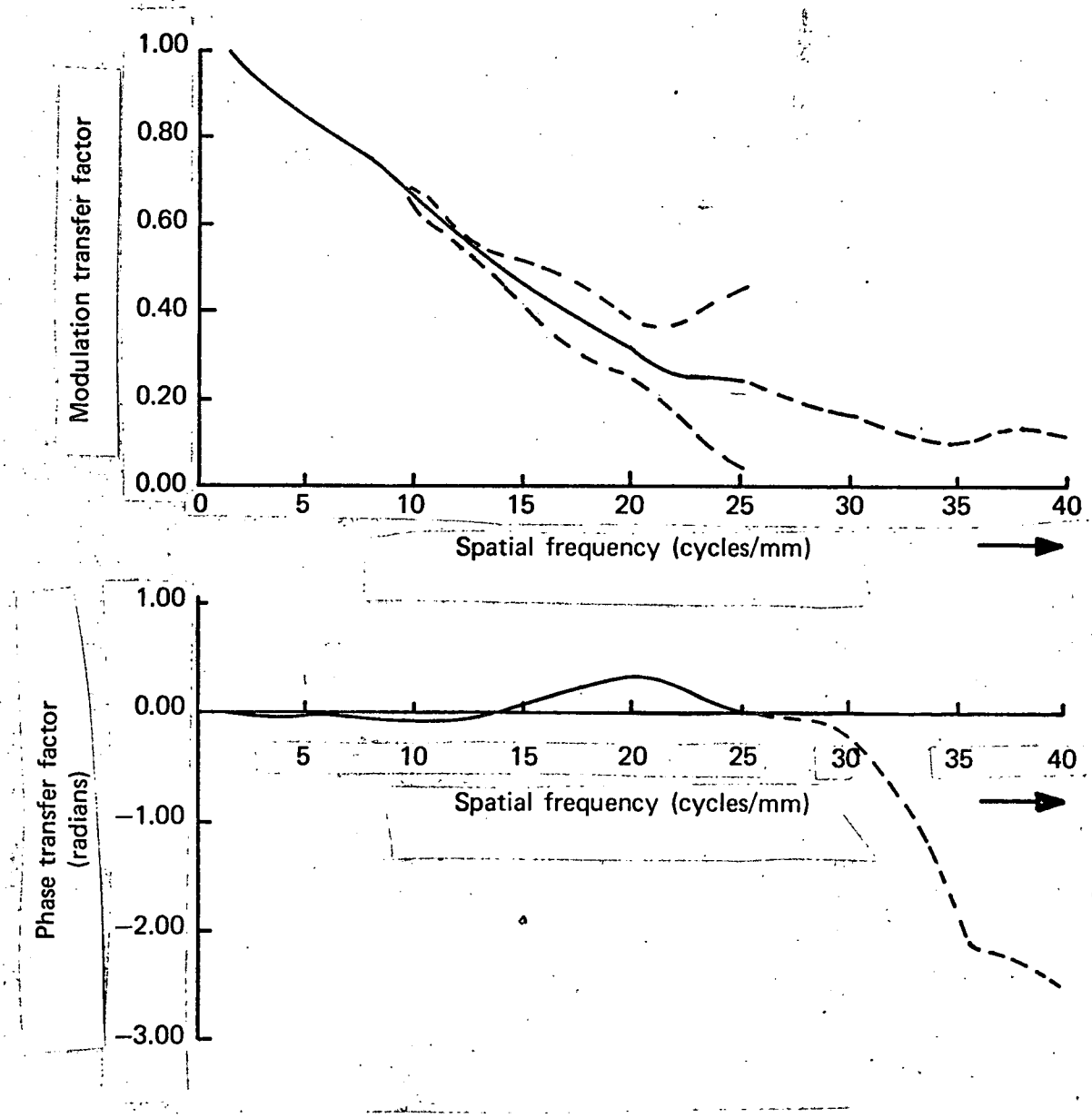

Fig. 5. S065 sensor (DD band) OTF